Egyptian Journal of Chemistry

Fabrication of hydroxyapatite–aluminum silicate/chitosan-gelatin biocomposites with *In-Vitro* application by preosteoblast cells (MC3T3-E1)

Khaled R. Mohamed*[a], Sahar Mousa[b], Bothaina M. Abd El-Hady[c], Emad Tolba[c], Gehan T. El Bassyouni[a]

[a] Refractories, Ceramics and Building Materials Dept., Biomaterials group, National Research Centre, 33 El-Buhouth St., Dokki, Cairo, 12622, Egypt
[b] Inorganic Chemistry Dept., National Research Centre, 33 El-Buhouth St.,Dokki, Cairo, 12622, Egypt
[c] Polymers and Pigments Dept., National Research Centre, 33 El-Buhouth St., Dokki, Cairo, 12622, Egypt

Abstract

Hydroxyapatite (HA) was widely used in tissue engineering, because of its excellent biocompatibility and biological activity. In this study, HA powder was modified using amorphous aluminosilicate (AAS). HA/AAS hybrids were synthesized via a wet precipitation method. Composites of HA–AAS/chitosan–gelatin polymer were prepared and characterized using X-ray diffractometry, Fourier-transform infrared spectroscopy, transmission electron microscopy, scanning electron microscopy, pore size distribution, and surface area measurements. The results show that HA with a rod-like structure and sheets of AAS were connected via a chitosan–gelatin network in the formation of the composites, leading to high reduction in their specific surface area due to polymer coating. Biocomposites with lower content of AAS nanoparticles exhibited a compressive strength in the range of 3.1 to 7.3MPa and Young's modulus in the range of 0.11 to 0.21GPa, which were located within the range of human cancellous bone that have the range of 2–12 MPa and 0.05–0.5GPa, respectively. The bioactivity study proved that the composites samples enhance proliferation of preosteoblast cells (MC3T3-E1) and exhibit a lower toxicity than powder samples. Such findings shed light on HA-AAS/ chitosan–gelatin composites, as multifunctional materials for use in cancellous bone applications in the future.

Keywords: Hydroxyapatite; Chitosan; Aluminum silicate; Toxicity; Bioactivity

I. Introduction:

The field of biomedical science has been at the forefront in the pioneering for use in both therapeutic and diagnostic applications. Hydroxyapatite (HA) is a naturally occurring mineral form of calcium apatite, with a structure and configuration close to that of nature bone mineral, making it an ideal material to use in bone tissue engineering owing to its excellent biocompatibility, osteoconductivity, and osteoinductivity [1]. HA has a unique capability of binding to the natural bone through biochemical bonding, which promotes the interaction between host bone and grafted material. Being a bioactive ceramic HA is widely used in bone tissue engineering [2-4]. The properties of HA are affected by the crystallinity, stoichiometry, and specific surface area.

However, HA are highly brittle and exhibit poor mechanical stability, which limit their applications in tissue engineering [5]. To overcome these problems, the development of polymer/bioceramics composites is essential. In addition, polymers can be used as binders in ceramics to reduce their brittleness [6]. Aluminum silicate is usually used in the biomedical applications, owing to its superior configuration and high strengthening ability. The unique properties of aluminosilicate ($Al_2Si_2O_5(OH)_4$) have also led to be used in numerous ways in biomedicine and nanomedicine, specifically in drug delivery, gene delivery, tissue engineering, cancer and stem cell isolation, and bioimaging [7]. Aluminosilicates have been recognized as potential drug carriers due to their biocompatibility, high surface to volume ratio**,** ion-

_____

exchange ability, and excellent chemical and mechanical stability under physiological conditions [8]. Also, aluminosilicate microspheres obtained by spray drying were investigated in prospect of their potential biomedical applications [9]. Chitosan contains primary amine groups, in addition to secondary hydroxyl groups, in its monomer; therefore, it can be chemically modified without any change in its degree of polymerization [10,11]. Chitosan has a blending and charging mediator for nano materials that has allowed the formation of composites. In addition, chitosan exhibits promising biological properties; it is non-toxic, shows mucoadhesiveness, is biocompatible, and, more significantly, is biodegradable [12]. For instance, chitosan promotes bone formation in bone tissue by boosting osteoblasts formation in addition to its ability to regenerate the connective tissue [13]. Gelatin which is a partial derived product of collagen comprised of Arg-Gly-Asp (RGD) sequences which is normally found in the ECM [14]. Therefore, it allows for cell adhesion, attachment, and cell spreading more easily in a biocompatible manner. Moreover, gelatin has low antigenicity, and therefore, it possesses vital information signals for various biological processes. It has been reported earlier that mixture of chitosan and gelatin effectively promotes cell differentiation and cell proliferation [15]. Therefore, the composites of HA and aluminum silicate in the polymeric medium could improve the mechanical properties and bioactivity [16]. Porous mixtures of aluminosilicate/calcium phosphate have been studied for biomaterials applications, where it formed with an organic polymeric constitution present amorphous zeolites because of their 3D network structure and present the ability to link to bone matrix [17].The novelty in this study is how to benefit the good properties of all selected materials as HA, AAS, chitosan and gelatin to produce good bio composites due to their bioactive properties, besides the preparation of hydroxyapatite from natural and sustainable source (calcite) which is economically important, this work represents a novel approach to develop multifunctional of materials. The aim of this work was to produce HA/amorphous aluminosilicate (AAS) composites via a wet method and to study the effects that different concentrations of HA and AAS have on the prepared composite blends with bioactive polymers in terms of their microstructure, mechanical, thermal and bioactive properties.
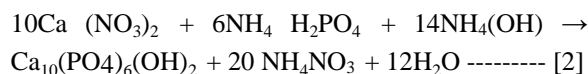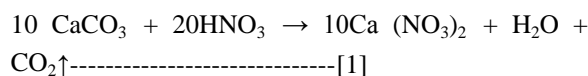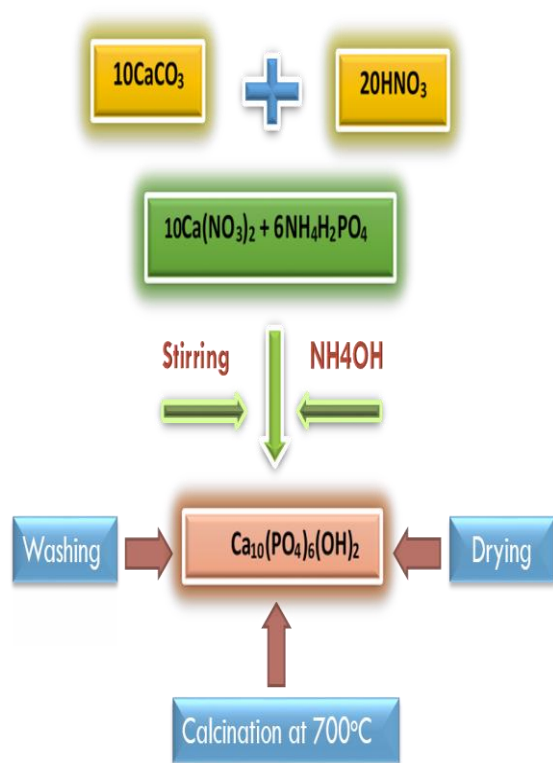
II. Materials and Methods
IIa. Materials

Egyptian calcite was used as a source of calcium. Diammonium hydrogen phosphate was purchased from Merck. Aluminum silicate (precipitated) was acquired from BDH, England. Chitosan (cationic polysaccharide, viscosity 800,000 cps) with a high molecular weight (M_r = 600,000) and an alkaline deacetylation of 85% was purchased from Sigma-Aldrich. Gelatin from porcine skin with a high purity of 99% was purchased from HAS HMRZEL Laboratories Ltd., Netherlands. Citric acid (CA, anhydrous 99%) was purchased from Morgan Chemical Ind. Co., Egypt.

IIb. Methods
b1. Preparation of HA

Because of its natural abundance as a raw material, calcite ore was used as a starting material for the preparation of nano-HA particles. 10 g of Calcite was ground and sieved (0.63 mm) before being mixed with distilled water. The calcite was then converted to calcium nitrate via the addition of nitric acid. Ammonium dihydrogen phosphate (6.9 g) was then added, and the pH was adjusted to 11 using ammonia solution (NH_4OH). The mixture was stirred for 2h at 40°C. To remove the ammonia, the $Ca_{10}(PO_4)_6(OH)_2$ was washed several times using distilled water and then dried at 100°C for 5h. The obtained powder was calcined at 700°C for 2h. The following equations and scheme show the method for the preparation of the hydroxyapatite:

$$10\ CaCO_3 + 20HNO_3 \rightarrow 10Ca\ (NO_3)_2 + H_2O + CO_2\uparrow \text{------------------------------}[1]$$

$$10Ca\ (NO_3)_2 + 6NH_4\ H_2PO_4 + 14NH_4(OH) \rightarrow Ca_{10}(PO4)_6(OH)_2 + 20\ NH_4NO_3 + 12H_2O \text{---------}[2]$$

_____

_____

Scheme of nano HA preparation by precipitation method.

b2. Preparation of HA/AAS powders

A series of chemical reactions were carried out to prepare HA/AAS materials with different ratios (1:1, 1:3, 3:1, and 5:1 of HA: AAS). After converting calcium nitrate to HA as mentioned before, the calculated amounts of AAS were dispersed in the solutions for 1h. The resultant mixtures were then washed using distilled water and then filtrated. The resultant products were dried at 100°C for 5h, before being calcined at 700°C for 2h.

b3. Preparation of HA/polymer composites
b3i. Preparation of HA/chitosan polymer composites

To prepare chitosan solutions, chitosan polymer (0.428 g) was dissolved in citric acid (CA) (15 mL of 4%, w/v) under stirring for 2 h at 40 °C to develop a gel solution [18]. HA powder (1.0 g) was added to the solution mixture, which was then well mixed, before being cast in a well plate to form cylindrical disks. Samples were dried at 40 °C for 48 h to obtain HA/chitosan polymer composites (**Table 1**). The interaction between HA and chitosan via hydrogen bonding between amino group of chitosan and

between the OH of HA and aluminosilicates materials occurred **[19, 20].**

3ii. Preparation of the HA/chitosan–gelatin polymer composites

Chitosan (0.285 g) and gelatin (0.143 g) were dissolved in 4% CA (15 ml) under stirring for 2 h at 40°C to form a gel solution. HA (1.0 g) powder was added, and the reaction mixture was well mixed before being cast in a well plate to obtain cylindrical disks. The well plate was placed in a dryer at 40°C for 48h to produce the HA/chitosan–gelatin composite (Table 1).

3iii. Preparation of the HA–AAS/chitosan–gelatin composites

Several experiments using the same steps and conditions as detailed in section (b2) were repeated employing various HA and AAS ratios (1:1, 1:3, 3:1, and 5:1, respectively), (HA:AAS) to prepare different HA–AAS/chitosan–gelatin composites as presented in Table 1.

Table 1: Abbreviation and meaning of the powder samples and their composites

Abbreviation	Sample
HA	um hydroxyapatite powder calcined at 700ºC
AAS	Amorphous aluminum silicate
1 : 1	1 HA : 1 AAS Powder
1 : 3	1 HA : 3 AAS Powder
3 : 1	3 HA : 1 AAS Powder
5 : 1	5 HA : 1 AAS Powder
HA / C	HA / Chitosan polymer composite
HA / CG	A / Chitosan - Gelatin polymer composite
1 : 1 / CG	1HA : 1AAS /Chitosan - Gelatin polymer
1 : 3 / CG	AAS / Chitosan – Gelatin polymer composite
3 : 1 / CG	AAS /Chitosan – Gelatin polymer composite
5 : 1 / CG	AAS / Chitosan – Gelatin polymer composite

c. In vitro cell culture

An appropriate cell model was used to study the biocompatibility of the materials. For cell culture and cell seeding, mouse calvaria cells, MC3T3-E1 cells (ATCC-CRL-2593; # 99072810; Sigma), were cultivated in minimum essential medium Eagle-alpha modification (αMEM, Gibco/Invitrogen, Darmstadt, Germany) containing 10% fetal calf serum (Gibco) **[21]**. The medium contained 2 mM L-glutamine, 1 mM sodium (Na) pyruvate, and 50 µg/mL of gentamycin. Cells were incubated in 25 ml flasks (Greiner BioOne, Frickenhausen; Germany) in

_____

an incubator at 37°C under atmosphere containing 5% CO_2. After reaching 70-80% confluency detachment (this is a standard protocol to prevent cell deformation and death), cells were detached using trypsin/EDTA and continuously subculture. Viability assays are important to estimate the cytotoxicity of nanoparticles against a specific cell type in which the cells are incubated with different concentration as reported before [22, 16].

The MC3T3-E1 cell line was inoculated with 1×10^4 cells per well (48 well plates (CLS3548; Sigma- Corning)) at a total volume of 0.5 mL [23]. The cultures were then incubated for two periods of 3 days. Subsequently, the PrestoBlue® cell viability assay was used, which functions as a cell viability indicator by reducing the power of living cells to quantitatively measure cell proliferation. Once added to cells, PrestoBlue® reduces the environment of viable cells and turns red, becoming highly fluorescent. This color change can then be detected via fluorescence or absorbance measurements [24].

The Presto Blue® cell viability reagent (Thermo Fisher Scientific, Waltham, MA, USA) was diluted 1:10 in phenol-free Dulbecco's modified Eagle medium before 1.5 ml of the diluted Presto Blue® solution was incubated with each sample for 4 h. The fluorescence signal of a 200 μl aliquot was detected using an excitation of 560 nm and an emission of 590 nm. Diluted PrestoBlue® reagent in the absence of cells or samples was used to measure the background fluorescence, which was then subtracted from the sample containing cells. In addition, the PrestoBlue® reagent was also incubated with the samples without cells to determine whether or not the samples interfere with the measurements. For cell imaging, cells seeded with the samples were stained using 5μM calcein–AM for 20 min at room temperature. Individual fluorescence images were captured using an Evos™ FL digital fluorescence microscope at an excitation wavelength of 494 nm and an emission of 540 nm.

d. Characterization

X-ray diffraction (XRD) patterns were recorded in reflection mode using an X-ray diffractometer (MiniFlex-600, Rigaku Corporation, Japan) over a scanning 2θ angle range of 10–70° at a scan rate of 10°/min. To determine the surface functional groups of the samples, Fourier-transform infrared (FT-IR,

Nicolet iS50, Thermo Fisher Scientific Ltd., USA) spectra were recorded over a wavenumber range of 4000-500 cm^{-1}. Brunauer–Emmett–Teller (BET) measurements were used to determine the specific surface area, adsorption–desorption, pore volumes, average pore diameters, and pore size distributions of the powders and their composites. A high-speed gas sorption analyzer (NOVA 2000 series, Chromatic, UK) was used to determine the nitrogen adsorption–desorption isotherms. Thermogravimetric analysis (TGA) of the prepared composite samples was carried out using a Shimadzu TGA-50 H apparatus under a flow of nitrogen gas (N_2) at a rate of 30 ml/min at 10°/min.

The prepared samples were suspended in distilled water, sonicated for one hour and dropped on copper grids supported by carbon film. The samples were then observed using transmission electron microscopy (TEM, JEM-2100F, JEOL Ltd., Japan). To study the crystal morphologies and microstructures of the prepared composites, scanning electron microscopy (FE-SEM, Model FEI, QUANTA FEG 250) measurements were carried out. Samples were sputtered with a thin film of gold prior to their imaging to ensure the capture of high-quality images. Acceleration voltage and the magnification of the SEM images were 30 KeV and 30000x, respectively.

e. Mechanical properties

The composites were also mechanically tested to determine the effects that the polymer and/or filler have on the mechanical properties of the composites. The compressive strength (CS) and Young's modulus (E) values were measured using a universal testing machine (Shimadzu 5 KN; Autograph AG-X Plus, Japan) at a cross-head speed of 1 mm/min and cell load of 5 kN . The CS was automatically calculated using a software (Trapezium X, Nexus 4000TM, Innovatest, model no.4503, Netherland) supplied by the machine. While the E value was calculated using the following formula: *F/A*, where *F* is the maximum stress and *A* is the cross-sectional area of the cylinder. Disk samples were prepared by pouring the mixed polymer/powder composites in molds and then dried at 40°C for 48h to obtain solid sample of diameter 1 cm and length 2 cm of a cylindrical shape. The same experiment was repeated to prepare three disk samples from each of the prepared composites for

measuring the CS and E properties. The average values for three samples (n=3) were taken for each composite to verify the mean value of the results.

III. Results and Discussion
a. Characterization
a1. XRD analysis

Fig.1 shows XRD patterns of Egyptian calcite, which was used as a low-cost starting material in the synthesis of HA, wherein only a pure phase of calcite [JCPDS (88-1808)] can be observed. XRD patterns of HA synthesized from calcite and dried at 100°C for 2 h show that it exhibits poor crystallinity. After calcination at 700°C for 2h, pure phase of HA material with high crystallinity was formed where the XRD pattern indexes the main peaks related to HA that was observed as sharp and narrow peaks which proved that the obtained material was in a crystalline phase [JCPDS (76-0694)].

Fig.2 shows XRD patterns of AAS and mixed HA and AAS powders with different HA: AAS ratios (1:1, 1:3, 3:1, and 5:1). Owing to its amorphous nature, AAS would be observed in the patterns as a characteristic hump-like peak. For all of the mixed HA/AAS samples, characteristic peaks of HA were observed at 25.8°, 28.2°, 29.1°, 31.9°, 32.3°, 33.1°, 34.2°, 40°, 47°, and 49°, corresponding to the (002), (102), (210), (211), (112), (300), (202), (130), (222), and (213) planes of the materials, respectively, **[25, 26].** Owing to its amorphous nature and being covered by HA nanoparticles, the patterns of all of the samples had not feature any signals that could be attributed to AAS. The mixing of the HA and AAS powders had an adverse effect on the crystallinity of HA, which reduced upon an increase in the amount of AAS present in the sample to 1:3 (HA:AAS), whereas the best crystallinity of all powder mixtures was that of the 5:1 HA:AAS sample, owing to its high HA content.

Fig.3 shows XRD patterns of the HA/C, HA/CG, and HA:AAS/CG composites prepared using different ratios of the reagents (1:1/CG, 1:3/CG, 3:1/CG, and 5:1/CG (HA:AAS/CG)). It was found that the characteristic peaks of HA were highly intense in the pattern of the calcined HA, but the intensity of these peaks started to reduce by the addition of the chitosan and gelatin polymers. Furthermore, the reduction in the intensity of the HA peaks increased for the 1:1/CG composite, reaching

the maximum for the 1:3/CG composite owing to the amorphous structure of the AAS powder, which shows its high affinity for polymer sites due to a high coating effect. However, the intensity of the peaks increased upon an increase in the HA content into the 3:1/CG composite and the intensity was more increased for the 5:1/CG composite, this indicates that HA was successfully introduced into the HA:AAS/CG composites [27].
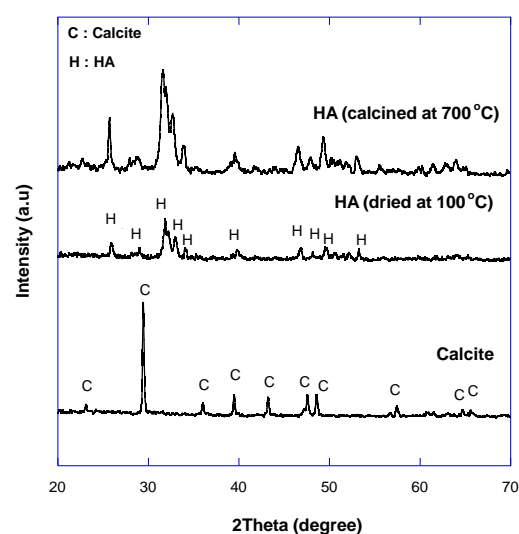

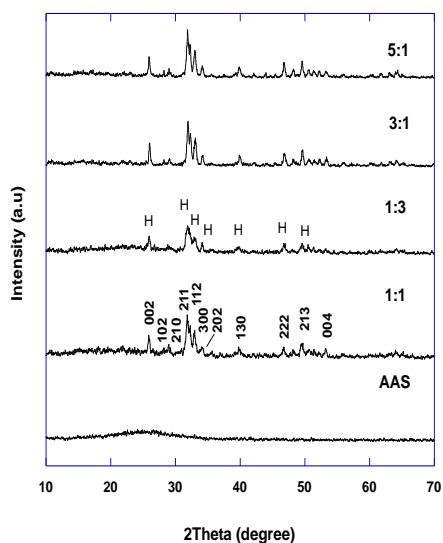**Fig. 1**: XRD patterns of natural calcite HA dried at 100°C and calcined at 700°C

Fig. 2: XRD patterns of HA and their mixed powders with AAS powder with different ratios (1:1, 1:3, 3:1 and 5:1)
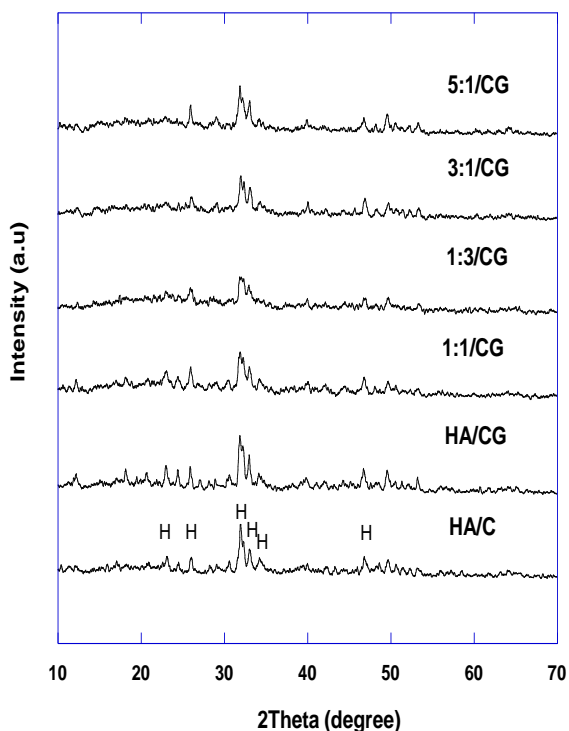

Fig.3: XRD patterns of HA/C, HA/CG and HA: AAS/CG composites with different ratios (1:1/CG, 1:3/CG, 3:1/CG and 5:1/CG).

a2. FT-IR analysis

Fig.4 shows the FT-IR spectra of the materials prepared in the current study. **Fig.4a** shows the spectra of HA, AAS, and their mixed powders. For HA, the intense bands in the region of 560–600 cm^{-1} can be ascribed to the v_4 bending of PO_4^{3-} and those in the region of 1000-1100 cm^{-1} to the v_3 bending of PO_4^{3-}. The peak at 1460 cm^{-1} can be attributed to CO_3^{2-}, which is present in the spectrum owing to the entrapment of atmospheric carbon dioxide during the preparation of the material [28]. A broad peak centered at 3441 cm^{-1} can be ascribed to the O–H stretching vibration mode and the band at 1640 cm^{-1} denotes the H–O–H bending vibration [29, 30]. The spectrum of AAS exhibits a band within the range of 1055-1000 cm^{-1}, which can be attributed to Si–O stretching vibrations in the silica, as well as Al–OH symmetric stretching vibrations, suggesting the presence of AAS, which fit into the SiO_4 and AlO_4 tetrahedra of the AAS in addition to the O–H stretching and bending vibration modes.
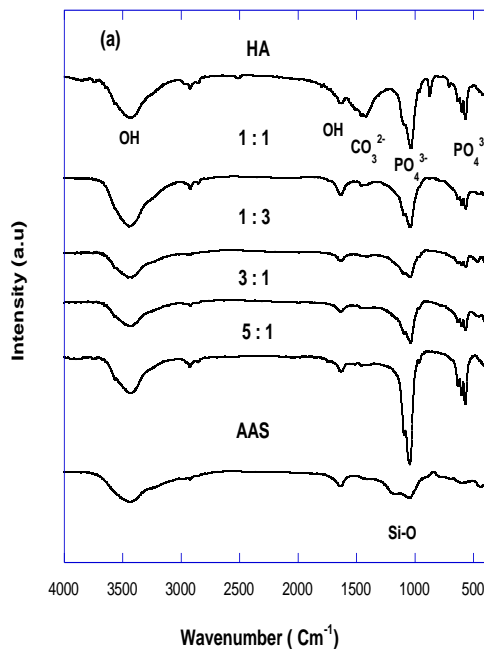

Fig.4a: FT-IR spectra of HA, AAS and their mixed powders with different ratios (1:1, 1:3, 3:1 and 5:1).

_____

For the HA:AAS mixed powder samples with 1:1, 1:3, 3:1, and 5:1 ratios, it is clear that the 5:1 HA:AAS sample shows the most intense characteristic peaks for HA compared with the other samples, owing to the high percentage of HA in the mixture [5]. Thus, this demonstrates that HA is uniformly distributed on the outside of the amorphous aluminum silicate plates (AAS) [31–33]. The large surface area of AAS, positively charged $Al(OH)_3$ on its inner surface and its negatively charged outer surface increase the probability of AAS satisfactorily binding with HA [34], as in the 1:3 HA:AAS composite.

Fig.4b shows the spectra of the HA/AAS/polymeric composites, wherein the broad peak centred at 3440 cm⁻¹ can be attributed to N–H stretching and –OH group stretching vibrations and the intermolecular hydrogen bonding of HA and the chitosan polymer [35]. The bands in the range of 1640–1620 cm⁻¹ correspond to the H–O–H bending vibration and C=O stretching, attributed as amide I, whereas the band at 1445 cm⁻¹ can be assigned to CH_2 bending vibrations [36-38]. In the spectra of the HA/C composite, the HA bands are still present, even after the loading of chitosan, but their optical density is reduced in comparison with that of pure HA (**Fig.4a**), demonstrating the effect of coating with the chitosan polymer on these sites. In the spectrum of the 5:1/CG composite, the C=O and C–H/amide I peaks are present at 1622 and 1445 cm⁻¹, respectively, attributed to the gelatin structure, whereas the amide I peak is present at 1445 cm⁻¹, attributed to chitosan [39]. The 5:1/CG composite shows intense peaks, thus indicating that HA was successfully introduced into the HA:AAS/CG composite. This result is in good agreement with the XRD results. It should be noted that the combination of AAS and HA loaded on the polymer showed high affinity to the polymer compared with the HA/C or HA/CG polymer composites, with this being due to the amorphous nature of AAS.
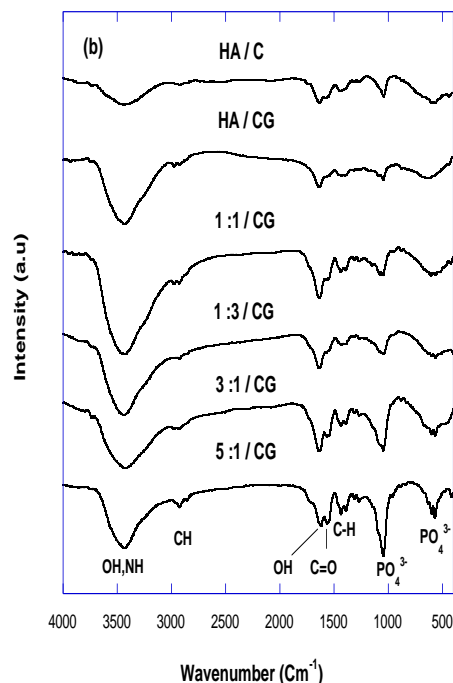

Fig. 4b: FT-IR spectra of HA/C, HA/CG and HA: AAS/CG composites with different ratios (1:1/CG, 1:3/CG, 3:1/CG and 5:1/CG)

a3. TGA analysis

Fig.5 shows TGA thermograms in the temperature range of 30-1000 °C and the total mass loss data of the prepared composites, from which the range of the stability of the composite upon an increase in temperature can be determined. Absorbed water in the range of 25–200 °C and structural (intra-crystalline) water in the range of 200–450 °C were observed to be lost from the composites. The largest total mass losses, of 38%, 36%, and 30%, were observed for 1:3/CG, 1:1/CG, and HA/CG, respectively, whereas a little mass loss value of 15% was observed for the HA/C composite (**Table 2**). These results provide evidence that the attachment of the chitosan–gelatin polymeric layer on the HA particles was greater than that of the chitosan polymeric layer and proving that the polymeric layer with attached HA nanoparticles decomposed with the release of structural water molecules at 345 and 540°C. The decomposition of polymeric layer completely released at 800°C [40]. Also, the effect of the amorphous nature of AAS decreased the

_____

thermal stability of the prepared composites upon its increase. The smallest total mass losses were 13% and 10%, observed for the 3:1/CG and 5:1/CG composites, respectively, which prove that an increase in the HA content leads to an increase in the thermal stability of both materials.

Table. 2: Total mass loss % values of the prepared composites

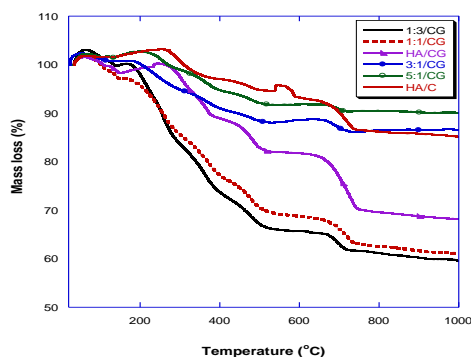| Compos ite	HA/ C	HA/C G	1:1/C G	1:3/C G	3:1/C G	5:1/C G
Mass loss %	15	30	36	38	13	10

Fig.5: TGA curves of the composites

a4. Surface area analysis

The BET specific surface areas of HA, AAS powders and their mixtures are listed in Table 3. It is clear from the data that an increase in the HA content at the expense of AAS reduces the surface areas of the mixtures, which is in good agreement with the results of a study by Zheng et al. [7]. Table 3 indicates the maximum adsorption and desorption values of HA, AAS, and their powder mixtures. The adsorption and desorption are low for HA, owing to it having a low surface area, and high for AAS, owing to it having a high surface area [41]. For the HA:AAS sample with a HA:AAS ratio of 1:3, a small amount of HA is distributed outside the AAS nanoparticles; thus, its adsorption performance and surface area are greater than those of pure AAS nanoparticles, which proved that nanoparticles (HA) are incorporated with a much lower size of material [42]. By contrast, in the case of HA: AAS samples with HA: AAS ratios of 3:1 and 5:1, a large number of the HA nanoparticles are located outside

the AAS, instigating the blockage of some of the AAS pores and the aggregation of some HA nanoparticles, consequently leading to a decrease in the surface areas and adsorption and desorption properties of these materials [16]. The total pore size distributions were observed to gradually decrease with an increase in the HA content, as in the HA/AAS (3:1) and HA/AAS (5:1) samples, and increase with an increase in the amount of AAS, as in the HA/AAS (1:3) sample (Table 3). All of the samples show a mono-modal pore size distribution in the pore size range of 2–10 nm. Therefore, the results indicate that HA/AAS mixtures were successfully prepared and that HA does not completely cover the surface of the AAS particles (plates) [43]. In this domain, intensive research over the past years has shown that nanostructured materials, characterized by dimensions of less than 100 nanometers, are indeed promising for a medical application [44]. As such, nanostructured materials are developed or applied as carriers for targeted drug and gene delivery [45]. In addition, Wang et al. [46] reported that nano porosity is known to impact the performance of implants. They prove that in vitro tests performed with MC3T3-E1 preosteoblast cells on such scaffolds show that initial cell attachment is increased on samples with the smaller nanopore size, providing the first direct evidence of the influence of nanopores topography on cell response to a bioactive structure.

Table 3: Textural characteristics of the prepared powders

Notati on of powder	Mean pore size (nm)	Total pore volume $(cm^3 g^{-1})$	Max. adsorpt ion ml/g	Max. desorpti on ml/g	Surface area $(m^2 g^{-1})$
HA	7.40	0.032	20.45	18.03	17.01
AAS	6.63	0.124	79.81	76.49	74.50
1:1	7.34	0.081	52.23	45.98	44.01
1:3	6.92	0.283	182.94	178.11	163.66
3:1	10.46	0.044	28.45	25.95	30.90
5:1	5.70	0.028	18.16	14.78	10.75

For surface area of composites, **Table 4** lists the BET specific surface areas of the HA, AAS, and

_____

their composites with polymers. It is clear from the data that for all of the composites samples, the loading of the powders onto the chitosan–gelatin polymeric materials led to a reduction in the surface areas compared to those of HA, AAS, and the HA/AAS powders as a result of the effect of coating the surface of the particles with polymer. The adsorption values of composites are low as they have a low specific surface area as a result of the polymer coating which led to the aggregation of the nanoparticles and an increase in particle size [16]. The total pore size distributions of all of the powders/polymeric composites were found to be decreased to a great extent compared with those of the powders as a result of the effect of the polymer coating, thus reducing the total pore sizes of the composites, as in 1:1/CG and1:3/CG, which contain a lower HA content than does the 3:1/CG composite. For the other composites, it is noted that the total pore size distributions are increased to a great extent,

especially those containing only HA nanoparticles on their structure, as in the HA/C and HA/CG composites, and also materials that contain the highest HA content, such as the 5:1/CG composite, due to the absence of AAS or a reduction in its content. Accordingly, all mean pore sizes increased for all prepared HA composites compared with those of the prepared powders samples that proved the presence of polymer improved the pore size distribution within the composites. In addition, all surface area, desorption and adsorption values decreased for all prepared HA composites compared with those of the prepared powders samples proving coating of polymer on these nanoparticles. In this domain, the absorption and desorption on HA were affected by the surface conditions dependent on the preparation procedure of HA[47], in fact, despite numerous studies suggesting the impact of nanostructure on cell function in various materials [48, 49].

Table 4: Textural characteristics of the prepared composites.

Notation of composites	Mean pore size (nm)	Total pore volume (cm^{3}g^{-1})	Max. adsorption ml/g	Max. desorption ml/g	Specific surface area (m^{2}g^{-1})
HA / C	11.17	0.025	16.26	6.92	9.01
HA / CG	15.98	0.026	16.71	5.32	6.47
1 : 1 / CG	8.65	0.029	19.00	10.05	13.6
1 : 3 / CG	27.16	0.017	10.80	3.97	2.46
3 : 1 / CG	15.96	0.042	26.94	13.54	10.45
5 : 1 / CG	6.08	0.014	9.32.	7.31	9.49

a5. TEM Analysis

Fig. 6a shows the TEM micrograph of HA powder, wherein it can be seen that the particle size distribution features a combination of morphologies of spherical agglomerates and globules [50]. The small dimensions of the HA crystal, along with its high surface area, promote its interaction with chitosan molecules [51]. For the AAS powder, **Fig. 6b** shows its TEM image, from which it can be observed that the material features bulk sheets that are large and smooth, formed from small sheets, where the width of these sheets is 23 nm [52]. For the HA/CG composite, it can be seen from the TEM image shown in **Fig. 6c** that the HA–chitosan/gelatin composite powder features a well-dispersed network of interconnected pores of different particle sizes of HA nanoparticles of 14–33 nm [53]. For the 1:3/CG

composite, the TEM image shown in **Fig.6d** confirms the presence of HA nanoparticles on the AAS. It can be seen that the HA/AAS mixture is distributed throughout the CG matrix, with it having the effect of reinforcing the CG. For the 5:1/CG composite, the TEM image shown in **Fig.6e** indicates the high HA content of this material, suggesting that it is mostly distributed on the outer surface of the AAS. Consequently, the aggregation of HA nanoparticles can be reduced by the integration of AAS. In this regard, Zheng et al., [16] stated that the smaller the size of the nanoparticles, the greater their surface energy. Accordingly, it was shown that the accumulation of HA nanoparticles can be altered via the incorporation of aaluminum silicate nanoparticles.
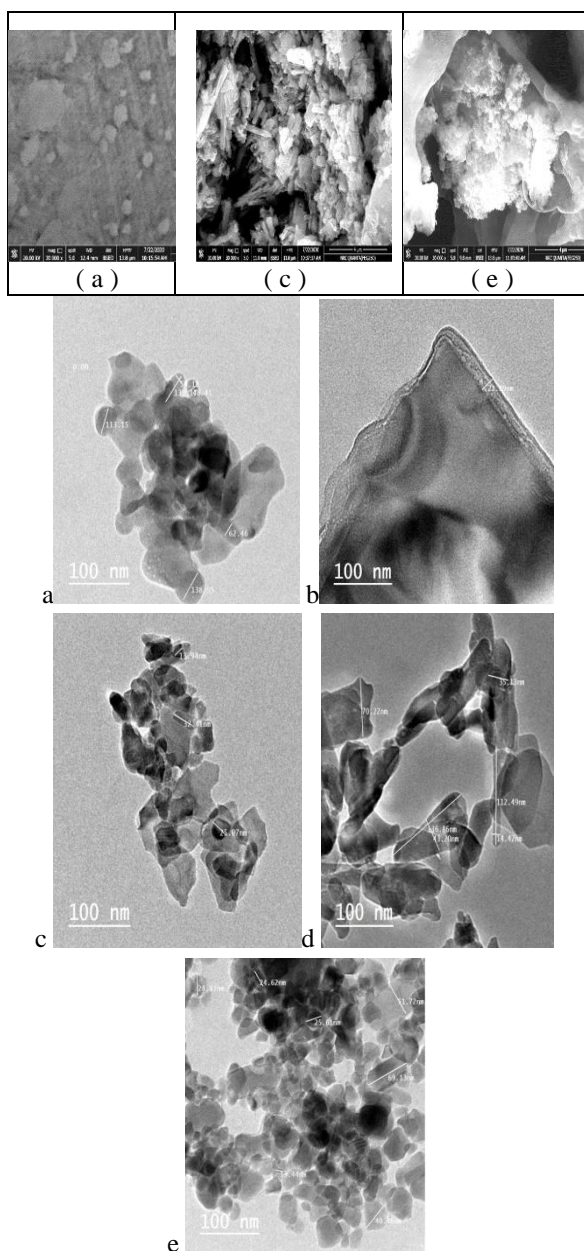
_____

Fig. 7B(b) shows the presence of HA particles surrounded by chitosan and gelatin polymers mixture with existence of many pores due to gelatin polymer effect within the composite [**55, 56**]. Likewise, its EDX prove the presence of calcium, phosphorus and oxygen as displayed in **Fig.7B(b)** thus confirming the presence of HA as well as polymers and these results agree with the XRD and FT-IR data. For 1:1/CG composite, **Fig.7A(c)** designates the presence of many plates and hexagonal shapes because of the adhering HA of particles on the AAS plates into the composite by polymers as binder with the occurrence of some pores on the surface **[57].**

Fig.7A: SEM images of (a) HA/C, (c) 1:1/CG and (e) 3:1/CG composites
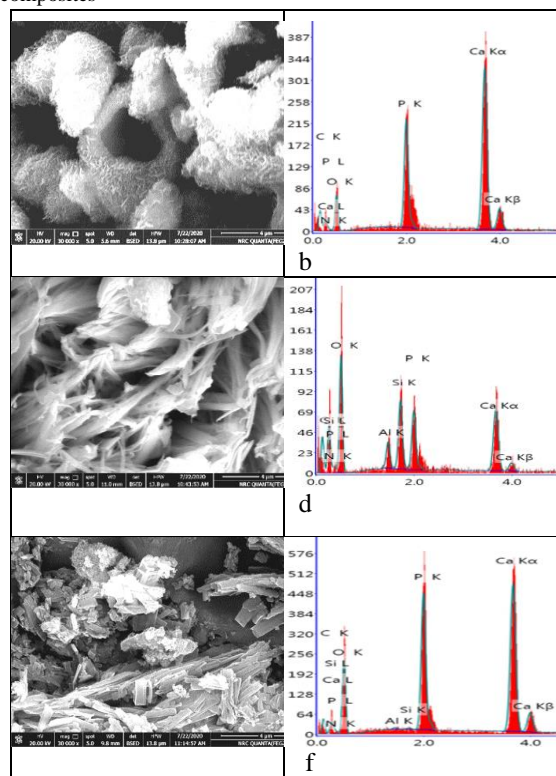

Fig.7B: SEM images and its EDX of (b) HA/CG, (d)1:3/CG and (f) 5:1/CG composites.

For 1:3/CG composite, **Fig.7B (d)** shows the presence of many plates of AAS connected together by polymers and few HA particles spread on their surfaces because of the increment of AAS content at the expense of HA content, Correspondingly, EDX confirms the presence of HA and AAS particles within the composite. For 3:1/CG composite, **Fig.7A (e)** exhibits a lot of HA particles connected,

Fig. 6: TEM micrographs of (a) calcined HA powder, (b) AAS powder (c) HA/CG composite, (d) 1:3/CG and (e) 5:1/CG composite.

a6. Surface morphology

The morphologies of the composites are shown in **Fig.7A and B**. For the HA/C composite, **Fig.7A(a)** exhibits the presence of HA particles implanted into the composite with the presence of a smooth surface proving coating by polymers because of the strong interaction between HA particles and chitosan via hydrogen bonding [**54**]. For the HA/CG composite,

_____

accumulated and agglomerated to each other by polymers with the appearance of few large pores as well as disappearance of AAS plates due to high content of HA particles into composite. For 5:1/CG composite, many HA nanoparticles agglomerated on plates of the AAS due to the higher content of HA proportion to polymer and its EDX proves that elements of HA, AAS and polymers were founded as elucidated in **Fig. 7B (f)**.

a7. Mechanical properties

Fig. 8 shows the compressive strength (CS) and Young's modulus (E) of the composites. It was clear that HA/C composite has the highest CS value due to the strong interactions between chitosan and HA [58]. The HA/CG composite shows a slight decrease in both CS and E values due to the attendance of gelatin, which has negative effect on its mechanical properties [59, 60]. A remarkable decrease in both CS and E values can be observed for the 1:1/CG composite and even more for the 1:3/CG composite due to the presence of the amorphous AAS phase with the HA. The decline in the mechanical properties are directly proportional to the increase in the amount of AAS present in the composites, with the opposite trend observed for the 3:1/CG and 5:1/CG composites, where the mechanical properties are improved upon an increase in the amount of HA in the composites at the expense of AAS. It is observed that the presence of nano HA material into the composite increase its mechanical properties due to its high crystallinity as shown in XRD despite the fact that AAS material has negative effect on the mechanical possessions by reason of its amorphous nature [61]. For human cancellous bone, CS and E values are in the range of 2–12 MPa and 0.05-0.5 GPa, respectively [62]. Consequently, agreeing to our results, all composites can be used as cancellous bone substitutes, especially those containing only nano HA as in HA/C and HA/CG composites, and these containing the highest nano HA content as in 5:1/CG composite and lowest AAS content in its structure. Additionally, the presence of nano HA powder with chitosan–gelatin mixture enhanced its mechanical properties compared with those for chitosan-gelatin hydrogels alone that have value 0.0033 GPa for Young's modulus and 2.15 MPa for a compressive strength [63].
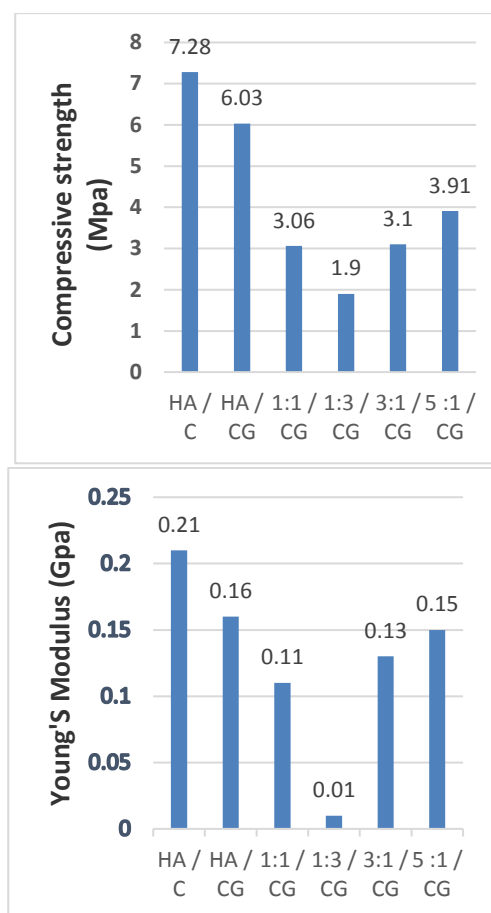

Fig.8: Compressive strength (CS) and Young's modulus (E) of the prepared composites. Data are evaluated as mean values ± SD for three experiments

b. In vitro cell culture
b1. Effect of powder samples on cell proliferation

To study the toxicity of the materials toward cells, MC3T3-E1 cells were cultured using complete culture medium with a certain amount of material to determine the activity of the cells. Cell viability is a common method that is used to monitor the response of cells in culture to materials by determining the number of growing (or survived) cells in the absence or presence of certain materials over a time period. To analyze the effects that the different samples have on cell growth, MC3T3-E1 cells were treated with different concentrations of the prepared samples (30, 100, 200, and 1000 µg/mL) for 3 days. **Fig. 9** shows the proliferation of MC3T3 cells grown on the various samples. For all of the tested samples, as the concentration of the material increases, the

cell activity decreases. This phenomenon can be explained by the fact that both AAS and HA/AAS are inorganic substances that tend to deposit at the bottom of the solution and affect the growth of the cells. At the same concentration, the cytocompatibility of HA/AAS is significantly better than that of pure AAS on account of the good biocompatibility of the HA nanoparticles [64]. Also, it was observed that there was a substantially higher level of growth of the cells treated with HA compared with the other samples. However, the HA/AAS samples exhibit acceptable levels of cell viability up to 30 and 100 μg/mL, while concentrations higher than 100μg/mL led to a significant reduction in the cell viability. This significant cytotoxicity potential may be attributed to the fast release of aluminum and (or) excessive generation of reactive oxygen species (highly reactive chemical molecules formed because of the electron acceptability of O_2), which in turn lead to an intrinsic apoptosis pathway due to oxidative stress [65]. Therefore, the HA/AAS samples should be used at high concentrations of up 100 μg/mL or be added to other polymeric materials to reduce the synergistic cytotoxic effect of combining HA and AAS nanoparticles in/at high concentrations. These results suggest that the cytocompatibility of AAS can be improved by anchoring it with HA nanoparticles, a result that has also been reported in a study by Zheng et al. [16].

Furthermore, the toxicity of the samples toward MC3T3-E1 cells was analyzed by fluorescence microscopy using calcein–AM (green) as a marker for living cells (**Fig.10**). The results confirmed the toxic effect of the AAS sample compared with HA and HA/AAS mixed samples, as a result of the toxicity of aluminum ions, especially in samples with high concentrations of AAS nanoparticles. In this context, Murphy et al. reported that aluminum silicate-containing clays promote the rapid lysis of primary neuronal cells *in vitro* [66]. The AAS sample showed significant toxicity, even at low concentrations, whereas the HA sample did not affect the cell viability. The combination of HA and AAS in different ratios as powder samples (1:5, 1:3, 1:1, and 1:3) exhibited a concentration-dependent toxic effect, with the values expressed as the percent of viable cells cultured in the absence of the samples (mean ± standard deviation).
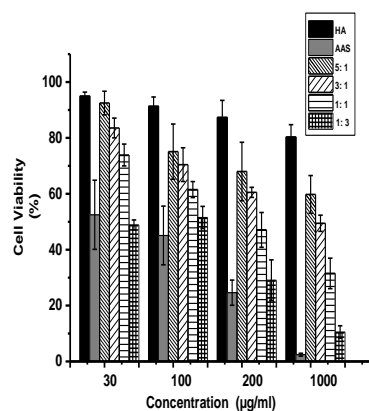

Fig. 9: Toxicity of the different powders samples in MC3T3-E1cell line after 3 days. Data are evaluated as mean values ± SD for three experiments.
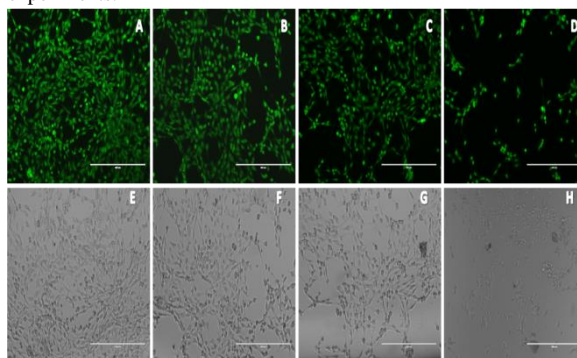

Fig.10: Fluorescence and light microscope images showing the results of calcein staining after 3 days of culture with powder samples at a concentration of 100 μg/ml (A, E) HA powder, (B, F) 5:1 powder, (C, G) 1:1 powder and (D, H) AAS powder.

b2.Effect of the composite samples on cell proliferation

It can be seen that after 3 days the HA/C exhibits lower cell viability than the HA/CG composite, which might be due to the adsorption properties of gelatin as a result of its electrostatic and/or hydrophobic nature, which is dependent on the surface and medium conditions [67] as revealed in **Fig. 11**. In contrast, after 3 days, the HA-AAS/CG shows significant cell viability, even at high concentrations, due to the presence of a certain concentration of AAS. Moreover, fluorescence microscopy was also used to observe the growth of cells after their incubation with calcein for 3 days, the results of which are shown in **Fig. 12**. Overall, the

cell viability (survival of the cells) was clearly observed in a dose-dependent manner for all of the composite samples, especially for the HA/C and 5:1/CG composite samples, owing to the high reactivity of HA, which leads to osteoblast differentiation and growth [68]. Furthermore, the presence of citric acid as a cross linker did not result in cytotoxicity even though it repaired normal proliferation rates 3 days after treatment, especially at the lowest concentration of (4%) [69]. The composites were found to enhance cell growth and exhibited reduced toxicity compared to the powders, thus proving the importance of the use of a polymer matrix, HA nanoparticles, and CA within the composites to enhance the bioactivity of the composites.
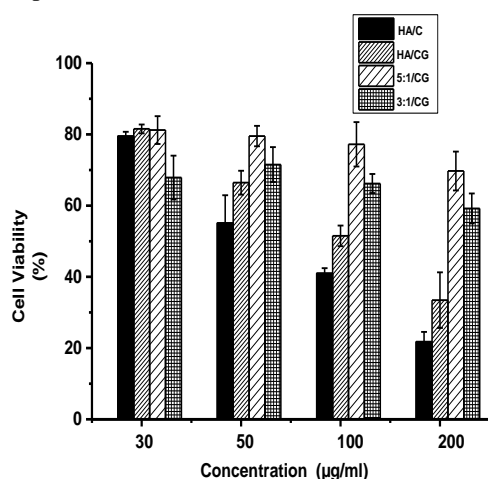

Fig. 11: Toxicity of different composites samples in MC3T3-E1cell line after 3 days. Data are evaluated as mean values ± SD for three experiments
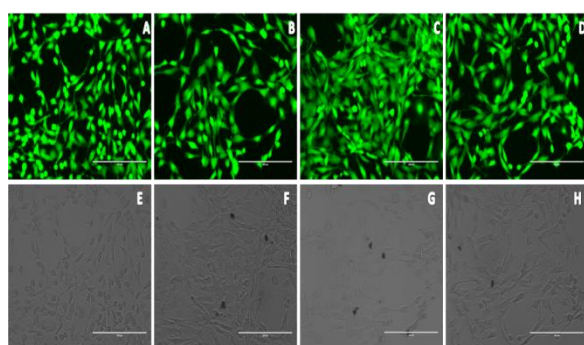

Fig. 12: Fluorescence and light microscope images show the results of calcein staining (green) after 3 days of culture with composite samples at a concentration of 50 μg/ml (A, E) HA/C, (B, F) HA/CG, (C, G) 5:1/CG and (D, H) 3:1/CG sample.

Conclusions

The current study specifies the characterization of HA and natural biopolymer composites concerning the development of composites materials for bone repair and regeneration. The results proved that the rod-like structure of HA and sheets of AAS, associated into composites via a chitosan-gelatin network, initiated a high reduction in the specific surface area of the composites. XRD data evidenced that by the addition of the chitosan/gelatin into the composites; there was a remarked reduction in the intensity of the XRD peaks. Nevertheless, the intensity of the peaks increased upon increment in the HA content thus signifying that HA was successfully presented into the HA:AAS/CG composite. TGA analysis verified that the increase in the HA content leads to an increase in the thermal stability of the 3:1/CG and 5:1/CG composites. Likewise; TEM image confirms the incidence of HA nanoparticles regularly dispersed on the outer surface of the AAS plates. Biocomposites with HA or HA-AAS with low AAS nanoparticles content exhibited a compressive strength of range from 3.1 to 7.3 MPa and Young's modulus of range from 0.11 to 0.21 GPa, which located within the range of human cancellous bone. The cell culture results evidenced that the composites improve cell growth and exhibit reduced toxicity compared to the powder samples, accordingly proving the importance of using a polymer matrix in the prepared biocomposites. Such findings shed light on /hydroxyapatite-AAS/ chitosan–gelatin composites, toward their use in biomedical applications. Besides, in vivo animal tests will be performed in the future to confirm the biomedical use of these biomaterials.

References

[1] S-t. Deng, H. Yu, Y-g. Bi, Ultrasonic-assisted Synthesis of Rod-shaped Hydroxyapatite Nanoparticles, International Forum on Energy,

Advances in Engineering Research, International Forum on Energy, Environment Science and Materials 120, 425-428 (2017).

[2] F. Scalera, F. Gervaso, K. P. Sanosh, A.Sannino, A. Licciulli, Influence of the calcination temperature on morphological and mechanical properties of highly porous hydroxyapatite scaffolds, Ceram.Int.39 4839–4846 (2013).

[3] M. Liu, Z. Jia, D. Jia, C. Zhou, Recent advance in research on halloysite nanotubes polymer nanocomposite, Prog Polym Sci 39, 1498-1525 (2014).

[4] G.T. El-Bassyouni, Regenerative medicine in Nanotechnology and Biomaterials" LAP LAMBERT Academic Publishing Saarbrücken, Germany ISBN-13: 9783659808562, (2015).

[5] A.N. Elboraey, H.H. Abo-Almaged, A.A. El-Ashmawy, A.R. Abdou, A.R. Moussa, L.H. Emara, G.T. El Bassyouni, M.I. Ramzy, Biological and mechanical properties of denture base material as a vehicle for novel Hydroxyapatite nanoparticles loaded with drug, Advanced Pharmaceutical Bulletin (APB) 11(1) 86-95 (2021).

[6] M.V. Jose, V. Thomas, K.T. Johnson, D.R. Dean, E. Nyairo, Aligned PLG/HA nano fibrous nanocomposites scaffolds for bone tissue engineering, Acta Biomater. 5(1), 305-315 (2009).

[7] N.A. Negm, H.H.H. Hefni, A.A.A. Abd-Elaal, E.A. Badr, M.T.H. Abou Kana, Advancement on modification of chitosan biopolymer and its potential applications, International Journal of Biological Macromolecules 152, 681-702 (2020).

[8] V. Grumezescu and A.M. Grumezescu, Materials for Biomedical Engineering Inorganic Micro and Nanostructures, Book (2019), eBook ISBN: 9780081028155.

[9] M. Todea, B. Frentiu, R.F.V. Turcu, P. Berce, S. Simon, Surface structure changes on aluminosilicate microspheres at the interface with simulated body fluid, Corrosion Science, 54, 299-306 (2012).

[10] K.R. Mohamed, G.T. El-Bassyouni, H.H. Beherei, Chitosan Graft Copolymers-HA/DBM Biocomposites: Preparation, Characterization, and *In Vitro* Evaluation, Journal of Applied Polymer Science 105, 2553-2563 (2007).

[11] G.T. El-Bassyouni, K.R. Mohamed, W.I. Abdel-Fattah, M.I Ramzy, A.M. Ramadan A. Sobhy, Endosseous dental implant using Aluminum Calcium Phosphate with and without Sugar Mediated Chitosan Membrane, Australian Journal of Basic and Applied Sciences 6(8), 645-653 (2012).

[12] W.S. Xia, P. Liu, J. Liu, Advance in chitosan hydrolysis by non-specific celluloses. Bioresour. Technol. 99, 6751-6762 (2008).

[13] Polo-Corrales, L.; Latorre-Esteves, M.; Ramirez-Vick, J.E. Scaffold design for bone regeneration. J. Nanosci. Nanotechnol. 14, 15–56 (2014).

[14] H. Nagahama, V.V. Divya Rani, K.T. Shalumon, R. Jayakumar, S.V/ Nair, S. Koiwa et al., Preparation, characterization, bioactive and cell attachment studies of alpha-chitin/gelatin composite membranes. Int J Biol Macromol 44:333–337 (2009)

[15] H. Nagahama, H. Maeda, T. Kashiki, R. Jayakumar, F. Furuike, H. Tamura, Preparation and characterization of novel chitosan/gelatin membranes using chitosan hydrogel. Carbohydr Polym 76:255–260 (2009).

[16] J. Zheng, F. Wu, H. Li, M. Liu, Preparation of bioactive hydroxyapatite @ halloysite and its effect on MC3T3-E1 osteogenic differentiation of chitosan film, Materials Science & Engineering C 105, 110072 (2019).

[17] H. Oudadesse, A.C. Derrien, S. Martin, H. Chaair, G. Cathelineau, Surface and interface investigation of aluminosilicate biomaterial by the in vivo experiments, Applied Surface Science 255(2), 593-596 (2008).

[18] Q.-X. Wu, D.-Q. Lin, S-J. Yao, Design of chitosan and its water soluble derivatives-based drug carriers with polyelectrolyte complexes, Mar. Drugs 12, 6236-6253 (2014).

[19] K.R. Mohamed and A.A. Mostafa, Preparation and bioactivity evaluation of hydroxyapatite-titania/chitosan-gelatin polymeric biocomposites, Materials Science and Engineering: C 28 (7), 1087-1099 (2008).

[20] K.R. Mohamed, H.H. Beherei, Z.M. El-Rashidy, *In vitro* study of nano hydroxyapatite/chitosan–gelatin composites for bio-applications. Journal of Advanced Research. 5(2), 201-208 (2014).

[21] N. Takahashi, A.P. Kimura, K. Ohmura, S. Naito, M. Yoshida, M. Ieko, Knockdown of long noncoding RNA dreh facilitates cell surface GLUT4 expression and glucose uptake through the involvement of vimentin in 3T3- L1 adipocytes. Gene 735 (Suppl 5), 144404 (2020).

[22] N. Lei, H. Mengjuan, W. Tianwen, S. Meng, H. Ruixia, Nanostructured selenium-doped biphasic

calcium phosphate with in situ incorporation of silver for antibacterial applications, Scientific Reports, 10(1), 13738 (2020).

[23] P. Rejmontová, Z. Capáková, N. Mikušová, N. Maráková, V. Kašpárková, M. Lehocký, P. Humpolíˇcek, Adhesion, Proliferation and Migration of NIH/3T3 Cells on Modified Polyaniline Surfaces, Int. J. Mol. Sci. 17, 1439 (2016).

[24] A. Schreer, C. Tinson, J.P. Sherry, K. Schirmer, Application of Alamar blue/5-carboxyfluorescein diacetate acetoxymethyl ester as a noninvasive cell viability assay in primary hepatocytes from rainbow trout, Anal Biochem 344, 76-85 (2005).

[25] K.R. Mohamed, H.H. Beherei, G.T. El Bassyouni, N. El Mahallawy, Fabrication and mechanical evaluation of hydroxyapatite/oxide nano-composite materials, Materials Science and Engineering C 33, 4126-4132 (2013).

[26] T.A. Kuriakose, S.N. Kalkura, M. Palanichamy, D. Arivuoli, K. Dierks, G. Bocelli, C. Betzel, Synthesis of stoichiometric nano crystalline hydroxyapatite by ethanol-based sol-gel technique at low temperature, J Cryst Growth. 263(1-4), 517-523 (2004).

[27] S. Yadav, P. Singh, R. Pyare, Synthesis, characterization, mechanical and biological properties of biocomposite based on zirconia containing 1393 bioactive glass with hydroxyapatite, Ceramics International Part A 46(8), 10442-10451 (2020).

[28] K.R. Mohamed, S.M.A. Mousa, G.T. El-Bassyouni, Fabrication of nano structural biphasic materials from phosphogypsum waste and their *in vitro* applications, Materials Research Bulletin 50, 432-439 (2014).

[29] H.H. Beherei, G.T. El-Bassyouni, K.R. Mohamed, Modulation, characterization and bioactivity of new biocomposites based on apatite, Ceramics International 34, 2091-2097 (2008).

[30] S.M.A. Mousa and A.A. Hanna, Synthesis of nano-crystalline hydroxyapatite and ammonium sulfate from phosphogypsum waste, Materials Research Bulletin 48, 823-828 (2013).

[31] A. Molaei, M.A. Yousefpour Electrophoretic deposition of chitosan–bioglass–hydroxyapatite–halloysite nanotube composite coating, Rare Met. Published Online 5 April (2018).

[32] S. Satish, M. Tharmavaram, D. Rawtani, Halloysite nanotubes as a nature's boon for biomedical applications, Nanobiomedicine 6, 1-16 (2019).

[33] R. Yendluri, D.P. Otto, M.M. De Villiers, Application of halloysite clay nanotubes as a pharmaceutical excipient. Int J Pharm 521, 267-273 (2017).

[34] A. Georgopoulou, F. Papadogiannis A. Batsali J. Marakis, K. Alpantaki, A.G. Eliopoulos, C. Pontikoglou, M. Chatzinikolaidou, Chitosan/gelatin scaffolds support bone regeneration, J Mater Sci Mater Med 29(5), 59 (2018).

[35] L. You, F. Lu, D. Li, Z. Qiao, Y. Yin, Preparation and flocculation properties of cationic starch/chitosan crosslinking-copolymer. J Hazard Mater, 172, 38-45 (2009).

[36] T.I.M. Ragab, G.T. El-Bassyouni, W.A. Helmy, H.A.A. Taie, A. Refaat, M.A. Ibrahim, E. Abd El-Hmeed, M.A. Esawy, Evaluation of Multifunction Bioactivities of Extracted Chitosan and their UV/Ozone Derivatives, Journal of Applied Pharmaceutical Science 8(10), 53-62 (2018).

[37] S.R.R. Rajasree, M. Gobalakrishnan, L. Aranganathan, M.G. Karthih, Fabrication and characterization of chitosan based collagen/ gelatin composite scaffolds from big eye snapper *Priacanthus hamrur* skin for antimicrobial and antioxidant applications, Materials Science & Engineering C 107, 110270 (2020).

[38] H.K. Tchakouté, S.J.K. Melele, A.T. Djamen, C.R. Kaze, E. Kamseu, C.N.P. Nanseu, C. Leonelli, C.H. Rüscher, Microstructural and mechanical properties of poly(sialate-siloxo) networks obtained using metakaolins from kaolin and halloysite as aluminosilicate sources: A comparative study, Applied Clay Science 186, 105448 (2020).

[39] A.M. Abu El-Soad, A.V. Pestov, D.P. Tambasova, V.A. Osipova, N.A. Martemyanov, G. Cavallaro, E.G. Kovaleva, G. Lazzara, Insights into grafting of (3-Mercaptopropyl) trimethoxy silane on halloysite nanotubes surface, Journal of Organometallic Chemistry 915, 121224 (2020).

[40] I. Yamaguchi, S. Iizuka, A. Osaka, H. Monma, J. Tanaka, The effect of citric acid addition on chitosan/hydroxyapatite composites, Colloids and Surfaces A: Physicochem, Eng, Aspects 214 (1-3), 111-118 (2003).

[41] L. Gu, X. He, Z. Wu, Mesoporous hydroxyapatite: Preparation, drug adsorption, and release properties, Materials Chemistry and Physics 148, 153-158 (2014).

_____

[42] R. Chen, J. Shi, B. Zhu, L. Zhang, S. Cao, Mesoporous hollow hydroxyapatite capped with smart polymer for multi-stimuli remotely controlled drug delivery, Microporous and Mesoporous Materials 306, 110447 (2020).

[43] K.S.W. Sing and R.T. Williams, Physisorption Hysteresis Loops and the Characterization of Nanoporous Materials, Adsorption Science & Technology 22(10), 773-782 (2004).

[44] M. Goldberg, R. Langer, X.Q. Jia, Nanostructured materials for applications in drug delivery and tissue engineering. J Biomater Sci Polym Ed 18(3), 241-268 (2007).

[45] L. Grausova, A. Kromka, Z. Burdikova, A. Eckhardt, B. Rezek, J. Vacik, K. Haenen, V. Lisa, L. Bacakova, Enhanced growth and osteogenic differentiation of humanosteoblast-like cells on boron-doped nanocrystalline diamond thin films, PLoS One 6(6), e20943 (2011).

[46] S. Wang, T.J. Kowal, M.K. Marei, M.M. Falk, H. Jain, Nanoporosity Significantly Enhances the Biological Performance of Engineered Glass Tissue Scaffolds, Tissue Engineering: Part A, 19(13-14), 1632-1640 (2013).

[47] C. Kojima and K. Watanabe, Adsorption and Desorption of Bioactive Proteins on Hydroxyapatite for Protein Delivery Systems, Journal of Drug Delivery Volume 2012, Article ID 932461, 4 pages (2012).

[48] M.J. Dalby, M.J.P. Biggs, N. Gadegaard, G. Kalna, C.D.W. Wilkinson, A.S.G. Curtis, Nanotopographical stimulation of mechanotransduction and changes in interphase centromere positioning. J Cell Biochem 100(2), 326-338 (2007).

[49] S.K. Misra, D. Mohn, T.J. Brunner, W.J. Stark, S.E. Philip, I. Roy, V. Salih, J.C. Knowles, A.R. Boccaccini, Comparison of nanoscale and microscale bioactive glass on the properties of P(3HB)/Bioglass composites, Biomaterials 29(12), 1750-1761 (2008).

[50] N.A.S. Mohd Pu'ad, P. Koshy, H.Z. Abdullah, M.I. Idris, T.C. Lee, Syntheses of hydroxyapatite from natural sources, Heliyon 5(5), e01588 (2019).

[51] K. Maji, S. Dasgupta, B. Kundu, A. Bissoyi, Development of gelatin-chitosan hydroxyapatite based bioactive bone scaffold with controlled pore size and mechanical strength, J Biomater Sci Polym Ed 26(16), 1190-209 (2015).

[52] G. Cerefice, L. Ma, M. Kaminski, Microscopic and Spectroscopic Characterization of Aluminosilicate Waste Form with Cs/Sr/Ba Loading Using Scanning Electron Microscopy, Transmission Electron Microscopy, and X-Ray Diffraction, Metallurgical and Materials Transaction A 40A, 2876-2887 (2009).

[53] K. Maji and S. Dasgupta, Hydroxyapatite-Chitosan and Gelatin Based Scaffold for Bone Tissue Engineering, Trans. Ind. Ceram. Soc. 73(2), 110-114 (2014).

[54] X. Shen, H. Tong, T. Jiang, Z. Zhu, P. Wan, J. Hu, Homogenous chitosan/carbonate apatite/citric acid nano composites prepared through a novel in situ precipitation method, Composites Sciences and Technology 67(11-12), 2238-45 (2007).

[55] S. Teng, L. Chen, Y. Guo, J. Shi, Formation of nano-hydroxyapatite in gelatin droplets and the resulting porous composite microspheres, Inorganic Biochemistry 101(4), 686-691 (2007).

[56] C. Shu, Y. Xianzhu, X. Zhangyin, X. Guohua, L. Hong, Y. Kangde, Synthesis and sintering of nano-crystalline hydroxyapatite powders by gelatin based precipitation method, Ceramics International 33(2), 193-196 (2007).

[57] M. Gruszczyński and M. Lenart, Durability of mortars modified with the addition of amorphous aluminum silicate and silica fume, Theoretical and Applied Fracture Mechanics 107, 102526 (2020).

[58] L. Mingxian, Z. Yun, W. Chongchao, X. Sheng, Z. Changren, Chitosan/halloysite nanotubes bionanocomposites: Structure, mechanical properties and biocompatibility, International Journal of Biological Macromolecules, 51(4), 566-575 (2012).

[59] K.R. Mohamed. Effect of Gelatin Content on Compressive Strength and Apatite Formation of nano-biocomposite materials, Part 1. Interceram 60(6), 376-378 (2011).

[60] L. Zhang, L. Yubao, Y. Apiing, P. Xuelin, W. Xuejiang, Z. Xiang, Preparation and in vitro investigation of chitosan/nano-hydroxyapatite composite used as bone substitute materials, Mater. Sci. Mater. Med. 16(3), 213-219 (2005).

[61] S. Siriluck, U. Zafar, C. Hare, A. Hassanpour, N.T. Lönnroth, N. Venugopal, M.T. Murtagh, M. Ghadiri, Influence of mechanical properties on milling of amorphous and crystalline silica-based solids, Powder Technology 391(10), 239-252 (2021).

_____

[62] L.L. Hench and J. Wilson, Introduction. In Advanced Series in Ceramics, Vol. 1, An Introduction to Bioceramics, McLaren M, Niesz DE (Eds), World Scientific: London (1993).

[63] Z. Shen, X. Cui, R. Hou, Q. Li, Tough biodegradable chitosan–gelatin hydrogels via in situ precipitation for potential cartilage tissue engineering, RSC Advances 5(69), 55640-55647 (2015).

[64] G.T. El-Bassyouni, S.S. Eldera, S.H. Kenawy, E.M.A. Hamzawy, Hydroxyapatite nanoparticles derived from mussel shells for *in vitro* cytotoxicity test and cell viability, Heliyon, 6(6), e04085 (2020).

[65] T. Heikkilä, H. A. Santos, N. Kumar, D. Y. Murzin, J. Salonen, T. Laaksonen, L. Peltonen, J. Hirvonen, V.-K. Lehto, Cytotoxicity study of ordered mesoporous silica MCM-41 and SBA-15 microparticles on Caco-2 cells, European Journal of Pharmaceutics and Biopharmaceutics 74, 483-494 (2010).

[66] E.J. Murphy, E. Roberts, D.K. Anderson, L.A. Horrocks, Cytotoxicity of aluminum silicates in primary neuronal cultures, Neuroscience 57(2), 483-90 (1993).

[67] C. Shu, Y. Xianzhu, X. Zhangyin, X. Guohua, L. Hong, Y. Kangde, Synthesis and sintering of nano-crystalline hydroxyapatite powders by gelatin based precipitation method, Ceramics International 33(2), 193-196 (2007).

[68] S.-S.Kim, M.S.Park, O.Jeon, C.Y.Choi, B.-S.Kim, Poly (lactide‐co‐glycolide)/hydroxyapatite composite scaffolds for bone tissue engineering, Biomaterials 27, 1399-1409 (2006).

[69] L.F. Guimarães, T.K. da Silva Fidalgo, G.C. Menezes, L.G. Primo, F.C. Silva-Filho, Effects of citric acid on cultured human osteoblastic cells, Oral Surg Oral Med Oral Pathol Oral Radiol Endod 110(5), 665-669 (2010).